Cancer Research

Metabolic Associations of Reduced Proliferation and Oxidative Stress in Advanced Breast Cancer

Livnat Jerby, Lior Wolf, Carsten Denkert, et al.

Cancer Res Published OnlineFirst September 17, 2012.

Published OnlineFirst on September 17, 2012; DOI:10.1158/0008-5472.CAN-12-2215

Integrated Systems and Technologies

Cancer Research

Metabolic Associations of Reduced Proliferation and Oxidative Stress in Advanced Breast Cancer

Livnat Jerby[1], Lior Wolf[1], Carsten Denkert[4], Gideon Y. Stein[2,3], Mika Hilvo[5], Matej Oresic[5], Tamar Geiger[2], and Eytan Ruppin[1,2]

Abstract

Aberrant metabolism is a hallmark of cancer, but whole metabolomic flux measurements remain scarce. To bridge this gap, we developed a novel metabolic phenotypic analysis (MPA) method that infers metabolic phenotypes based on the integration of transcriptomics or proteomics data within a human genome-scale metabolic model. MPA was applied to conduct the first genome-scale study of breast cancer metabolism based on the gene expression of a large cohort of clinical samples. The modeling correctly predicted cell lines' growth rates, tumor lipid levels, and amino acid biomarkers, outperforming extant metabolic modeling methods. Experimental validation was obtained *in vitro*. The analysis revealed a subtype-independent "go or grow" dichotomy in breast cancer, where proliferation rates decrease as tumors evolve metastatic capability. MPA also identified a stoichiometric tradeoff that links the observed reduction in proliferation rates to the growing need to detoxify reactive oxygen species. Finally, a fundamental stoichiometric tradeoff between serine and glutamine metabolism was found, presenting a novel hallmark of estrogen receptor $(ER)^+$ versus ER^- tumor metabolism. Together, our findings greatly extend insights into core metabolic aberrations and their impact in breast cancer. *Cancer Res; 72 (22); 1–9. ©2012 AACR.*

Introduction

The metabolism of cancer cells is fundamentally different from that of normal cells. The tumor's microenvironment, the activation of oncogenes, the need to avoid apoptosis, and high energetic demands—these are only some of the selective pressures that alter the metabolism of cells during carcinogenesis (1–3). Several recent studies have shown the involvement of metabolic remodeling in breast cancer (4–8). It has been recently shown that targeting metabolic genes hampers breast cancer tumorigenesis *in vivo* and that the key enzyme in serine metabolism, phosphoglycerate dehydrogenase (PHGDH), is exclusively essential for estrogen receptor negative $(ER)^-$ breast cancer (7). Further highlighting the heterogeneity of breast cancer metabolism, another study has recently shown that basal cells are glutamine auxotrophs, whereas luminal cells produce glutamine and secrete it (8). These findings show the potential clinical implications and importance of studying breast cancer metabolism. However, as yet, there is a dire lack of accurate flux rate and metabolite concentration measurements in cancer cells. In contrast, there are relatively ample genome-wide measurements of gene expression, both from cancer cell lines and from clinical samples. This gap creates a growing need to develop methods for approximating the metabolic phenotype based on transcriptomics or proteomics. Tackling this challenge to further elucidate the metabolic aspects of breast cancer, we present a novel computational method, termed metabolic phenotypic analysis (MPA).

The methodologic basis of MPA is constraint-based modeling (CBM), a genome-scale approach to study metabolism. CBM metabolic models have been shown to provide an appropriate context for analyzing high-throughput omics datasets and to elucidate the genotype to phenotype relationship (9). The approach has been extensively applied to study the metabolism of various organisms, from microbes (10–12) to humans (13, 14). The potential clinical use of modeling human metabolism has been previously shown across numerous studies, including the identification of hypercholesterolemia drug targets (9), reactions related to hemolytic anemia (9), and metabolic biomarkers of inborn errors of metabolism (15). Recently, a generic genome-scale metabolic model (GSMM) of cancer has been developed and used to predict selective drug targets by identifying synthetic lethal gene pairs (16). A cell line–specific GSMM of hereditary leiomyomatosis and renal cell cancer (HLRCC) has been developed to study this particular pathology. It predicted selective drug targets for HLRCCs

Authors' Affiliations: [1]The Blavatnik School of Computer Science, [2]The Sackler School of Medicine, Tel Aviv University, Tel Aviv; [3]Department of Internal Medicine 'B', Beilinson Hospital, Rabin Medical Center, Petah-Tikva, Israel; [4]Institute of Pathology, Charité Hospital, Berlin, Germany; and [5]VTT Technical Research Centre of Finland, Espoo, Finland

Note: Supplementary data for this article are available at Cancer Research Online (http://cancerres.aacrjournals.org/).

T. Geiger and E. Ruppin contributed equally as last authors.

Corresponding Authors: Livnat Jerby, School of Computer Sciences, Tel Aviv University, Tel Aviv 69978, Israel. Phone: 9723-6405378; Fax: 9723-9517681; E-mail: livnatje@post.tau.ac.il; and Tamar Geiger, Sackler School of Medicine, Tel Aviv University, Tel Aviv 69978, Israel. Phone: 9723-6405036; Fax: 9723-6407556; E-mail: geiger@post.tau.ac.il

doi: 10.1158/0008-5472.CAN-12-2215

Published OnlineFirst on September 17, 2012; DOI:10.1158/0008-5472.CAN-12-2215

that have been validated experimentally (17), showing the potency of studying cancer metabolism on a genome-scale. However, these studies, as many others, were based on data from cancer cell lines, which may fail to depict the metabolism of the cancer *in vivo*. Here, with the introduction and application of MPA, our study, based on data of clinical samples, provides a system-level view of breast cancer metabolism *in vivo*.

Materials and Methods

MPA

Given gene expression or protein abundance profiles, a set of metabolic processes (Supplementary Table S1), and a GSMM, MPA generates for each sample its metabolic profile as explained hereinafter. First, the expression of a gene or protein is defined as high or low, if it is α SD higher or lower than the mean expression of the genes or proteins within the same sample, respectively. Otherwise, it is considered moderate. In the current analysis, α was set to 0.5. Robustness analysis was conducted to ensure that the method is not sensitive to the selection of α (Supplementary Material and Supplementary Fig. S1).

On the basis of the gene–protein–reaction associations (9), this ternary gene or protein profile is transformed to reaction expression, as done in the work of Shlomi and colleagues (18). The expression of a reaction reflects the expression state of its enzymes or enzyme-encoding genes, if it is inferred from proteomics or transcriptomics, respectively. On the basis of the reaction expression profile, an MPA score is computed for each metabolic process. A metabolic process is defined by its medium (i.e., which metabolites can be secreted or absorbed) and its end-reaction, which often produces the target metabolite of that process. For example, for the process of gluconeogenesis from lactate, the medium is defined such that lactate is the only carbon source to produce glucose, and the end-reaction is the one that produces glucose. The medium is set by dividing the reactions that transport metabolites in and out of the cell, termed exchange reactions, into 3 groups: R_{secrete}, R_{uptake}, and R_{both}. R_{secrete} and R_{uptake} consist of exchange reactions that should only conduct secretion or uptake, respectively. R_{both} consists of all other exchange reactions. To constrain the model according to the medium, the constraints (A–C) are imposed:

$$0 \le v_i \le v_{\max},\ i \in R_{\text{secrete}} \quad \text{(A)}$$

$$v_i^{\min} \le v_i \le 0,\ i \in R_{\text{uptake}} \quad \text{(B)}$$

$$v_i^{\min} \le v_i \le v_i^{\max},\ i \in R_{\text{both}} \quad \text{(C)}$$

$$\beta \cdot v_{\text{end-reaction}}^{\max} \le v_{\text{end-reaction}},\ \beta \in [0,1] \quad \text{(D)}$$

where a positive (negative) flux through an exchange reaction denotes the secretion (uptake) of the metabolite, and v_i is the flux through reaction i, having $v_i^{\min}$ and $v_i^{\max}$ as its minimal and maximal feasible flux rates, respectively. Both $v_i^{\min}$ and $v_i^{\max}$ are found via flux variability analysis (FVA; ref. 19), applied considering the process at hand. A metabolic process is enforced to be active by constraining the lower bound of its end-reaction to be greater than its maximal feasible value found via FVA, times β, as shown in constraint (D). In the current analysis, β was set to 0.9. Robustness analysis was conducted to ensure that the method is not sensitive to this setting (Supplementary Material and Supplementary Fig. S1). The MPA score of a process P is Opt^*/Opt, where

Opt^* = the maximal fit to the expression under the medium constraints of P when enforcing P to be active, that is, under all the above constraints.

Opt = the maximal fit to the expression under the medium constraints of P, that is, under the constraints (A–C).

The fit to the expression is computed as the number of reactions whose activity is consistent with their expression state in a steady-state flux distribution that satisfies stoichiometric and thermodynamic constraints. It is found by formulating a mixed-integer linear programming (MILP) problem as defined in the work of Shlomi and colleagues (18). The MPA score is hence a value between 0 and 1. The higher it is, the more probability that the process is active. However, each process has a different bound to its minimal MPA score, which is determined by the number of reactions it depends on for its activity. If a given process depends on x reactions for its activity, then the lower bound of the MPA score of this process is:

$$Opt - x \le Opt^* \rightarrow \frac{Opt - x}{Opt} \le \frac{Opt^*}{Opt} = \text{MPAscore}$$

Therefore, the MPA values of a given process are treated as relative rather than absolute indications of the process' activity across different samples. The implementation of the MPA code in MATLAB is accessible through a Supplementary website (20). For a small-scale example of MPA's computation, see Supplementary Fig. S2.

Multiple hypothesis correction

As we conducted multiple tests to identify metabolic processes that differentiate between 2 clinical groups of interest, we corrected for multiple hypothesis testing via false discovery rate (FDR) to obtain FDR-corrected P, which are provided in the Supplementary Tables (21).

Reactive oxygen species detoxification score

The computation of the MPA reactive oxygen species (ROS) detoxification score was conducted by computing 2 MPA scores. One that denotes the capacity of the sample to consume superoxide and another that denotes its capacity to produce it. By dividing the former by the latter, we obtain the MPA ROS detoxification score.

Identification of metabolic biomarkers

A metabolic biomarker is a metabolite whose levels in the biofluids can differentiate between 2 clinical groups. Therefore, the candidate metabolic biomarkers are only metabolites known to be transported from the cell to the biofluids via

Published OnlineFirst on September 17, 2012; DOI:10.1158/0008-5472.CAN-12-2215

exchange reactions. The identification of metabolic biomarkers is done as follows:

(i) Given the gene expression or protein abundance profiles of 2 clinical groups G_1 and G_2.
(ii) Let B be the set of candidate biomarkers.
(iii) For each sample, $i \in G_1 \cup G_2$.
- For each metabolite, $j \in B$.
  - Compute the MPA scores v_{ij} and u_{ij}—that denote the capacity of sample i to secrete and uptake metabolite j, respectively.
  - Let $b_{ij} = v_{ij}/u_{ij}$.

(iv) For each metabolite, $j \in B$.
- Conduct Wilcoxon rank-sum test between $\{b_{ij} | i \in G_1\}$ and $\{b_{ij} | i \in G_2\}$.
- Let p_j be the obtained P value and record which of the groups (G_1 or G_2) obtained higher ranked scores.

(v) Correct for multiple hypothesis testing, using Bonferroni, FDR, or positive FDR (pFDR) correction.
(vi) Report the metabolites that obtained significant P values, following the correction (i.e., <0.05).

To identify amino acid biomarkers for breast cancer, we applied MPA to gene expression data from normal and cancer breast tissue (22–24). The predictions of metabolites were compared with a set of breast cancer amino acids biomarkers, compiled according to the analysis of measured plasma-free amino acids profiles of patients with breast cancer and controls (25). The significance of the accuracy between the predictions and the measurements was calculated by computing the empirical P values by randomly shuffling the predictions. To identify biomarkers for metastatic breast cancer, we applied MPA to gene expression profiles of breast cancer clinical samples (24).

Cell culture and proliferation experiment

HMT-3522-S1 cells and MFM223 were obtained from the ECACC; HCC2218 cells were obtained from the American Type Culture Collection; HCC1599, HCC1143, and HCC1937 cells were obtained from the German Collection of Microorganisms and Cell Cultures (DSMZ); and MCF10a and MDA-MB-453 were kindly provided by Axel Ullrich (Max-Planck Institute of Biochemistry, Martinsried, Germany). All cell lines that were purchased from cell banks were authenticated using short tandem repeat profiling. Stage III cells (HCC2218 and HCC1599) and stage II cells (HCC1143 and HCC1937) were grown in RPMI supplemented with 10% FBS. Precancerous cells MCF10a were cultured in Dulbecco's Modified Eagles' Media (DMEM):F12 supplemented with 5% horse serum, 20 ng/mL epidermal growth factor (EGF), 10 μg/mL insulin, 0.5 μg/mL hydrocortisone, and 0.1 μg/mL cholera toxin. Precancerous cells HMT-3522-S1 were cultured in DMEM:F12 supplemented with 250 ng/mL insulin, 10 μg/mL transferrin, 0.1 μmol/L sodium selenite, 0.1 nmol/L 17 β-estradiol, 5 μg/mL ovine prolactin, 0.5 μg/mL hydrocortisone, and 10 ng/mL EGF. Pleural effusion cells MDA-MB-453 were cultured in L-15 supplemented with 10% FBS and pleural effusion cells MFM223 were grown in MEM supplemented with 10% FBS. All cells were cultured with Pen/Strep and under 5% CO_2, except for MDA-MB-453, which were cultured under 0% CO2. All cells were tested negative for mycoplasma using PCR tests within 6 months before the experiments were carried out.

For determination of cell growth rate, cells were plated in hexaplicates in 96-well plates. During 5 days of the experiment each day, plates were centrifuged and fixed with 2.5% glutardialdehyde. Cells were stained with methylene blue followed by extraction of color with 0.1 mol/L HCl. Absorbance was measured at 620 nm. Experiments were carried out in 3 biologic replicates.

ROS measurements

MDA-MB-453, MFM223, HCC1937, and HCC1143 cells were stained with Mitosox (Molecular Probes; Invitrogen) according to the manufacturer's instructions. Quantitative measurement of fluorescence was conducted by fluorescence-activated cell-sorting analysis using FL2 filter and measurement of 10,000 cells per measurement. Experiments were carried out using 3 biologic replicates.

Results

MPA

Previous methods for incorporating contextual gene expression or protein abundance measurements within a generic CBM metabolic model have focused on describing the metabolic state by restricting the model to obtain an optimal fit to the data (18, 26–29). These approaches have shown much value in providing context-dependent metabolic descriptions. However, by requiring an optimal fit, they have ignored the ability of cells to adaptively reinstate lost functions by inducing even small changes in their overall gene expression. This, in turn, can potentially lead to false predictions of reaction inactivity and mask observed differences between metabolic states. In contradistinction, given a gene expression or protein abundance signature of a sample, MPA provides a genome-scale view of its metabolism by considering solutions that may deviate to some extent from the optimal fit–this yields an estimation of the *adaptive potential* of the sample to carry out an array of metabolic processes in a given context. In the model, a metabolic process is defined by its medium (i.e., which metabolites can be secreted or absorbed by the cell) and its end-reaction. On the basis of a curated, literature-based definition of metabolic processes (30), we assign each sample–process pair an MPA score (Fig. 1; Supplementary Fig. S2). First, the consistency of the sample molecular signature (mRNA expression, proteomics, as defined in ref. 18) with the metabolic state of the model is computed, when requiring the activation of the given process in its medium. Then, this consistency score is divided by the optimal consistency that can be obtained between the signature and the model under the same medium, without this additional activation constraint. The result is the final MPA score for this sample–process pair. It quantifies the extent of significant adaptive flux changes that are required to carry out the process examined,

Published OnlineFirst on September 17, 2012; DOI:10.1158/0008-5472.CAN-12-2215

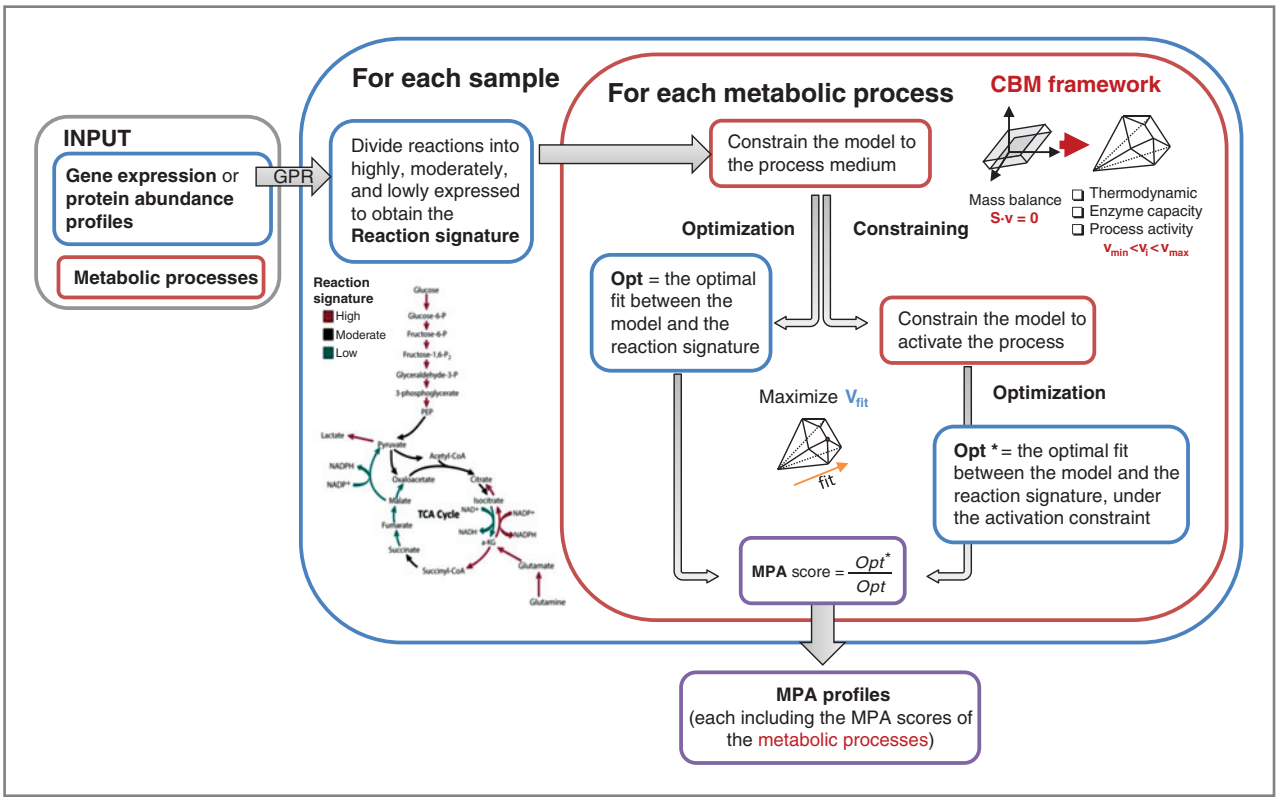

Figure 1. The MPA workflow. First, the gene expression or protein abundance profile of each sample is converted to a reaction signature according to the gene–protein–reaction (GPR) associations. The reaction signature consists of the expression state of each metabolic reaction (i.e., high, low, or moderate). Second, for each sample, an MPA profile is generated by assigning each metabolic process an MPA score that denotes its activity potential. This is done by solving 2 optimization problems that maximize the fit between the model and the reaction signature, with and without the constraint to activate the process. By solving these 2 problems, we obtain 2 unique fitness scores, whose ratio is the final MPA score of the process. The MPA profile of each sample is a collection of the MPA scores obtained for the different metabolic process that have been provided as input. The red and blue colors denote steps in which information about the metabolic process, or about the sample, are incorporated, respectively.

given the observed molecular signature (see Materials and Methods). A high MPA score (close to 1) denotes that a given process can be carried out in a given context with minimal adaptive flux or transcriptional changes and is hence more likely to occur, whereas a low MPA score (close to 0) denotes the opposite.

MPA validation

MPA was validated in 4 different ways. First, we examined the ability of MPA to capture known metabolic differences across 3 human tissues: muscle, liver, and adipose tissue (Supplementary Material and Supplementary Table S2). Second, we tested whether MPA can approximate the lipid production capacity of tumors. We used gene expression data to compute the capacity of 110 breast cancer tumors to produce lipids (31). The obtained lipid MPA scores were significantly positively correlated to the lipid measurements of these tumors (empirical $P = 6.40e\text{-}03$; Supplementary Material, Supplementary Fig. S3, and Supplementary Tables S3 and S4). Third, we computed MPA profiles of clinical breast cancer samples on the basis of their gene expression (24, 32) and used them to predict 5-year survival and metastasis-free survival via support vector machine (SVM) classifiers. For comparison, we built an array of alternative predictors: the gene expression of all genes, only metabolic genes, metabolic pathways enrichment features, and the expression of the genes included in the breast cancer prognostic signature identified by van't Veer and colleagues (ref. 32; Materials and Methods). The MPA-based predictors yielded a mean area under the curve (AUC) of 0.719, higher than those obtained by all other predictors (Supplementary Table S5). Improved performances were obtained by using the lipogenesis MPA profiles (with a mean AUC of 0.767). These results show the prognostic relevancy of MPA profiles, although prognosis prediction is not the prime goal of MPA, and not necessarily sufficient to validate a biologic model (33).

Finally, we show that MPA can bridge the gap between gene expression and protein abundance. MPA was applied to RNA-seq data of HeLa cells (34) to predict the activity state of the metabolic reactions (Supplementary Material). To study the performance of MPA, we tested predictions of posttranscriptional flux activity that do not arise directly from the gene expression input against the proteomics of these cells (34). That is, we focused on reactions in which the gene expression and predicted (flux) activity state differ (e.g.,

Published OnlineFirst on September 17, 2012; DOI:10.1158/0008-5472.CAN-12-2215

gene expression is low but the reaction is predicted to be active) and examined whether in these cases the prediction fits the proteomic data. Reassuringly, reactions that were predicted as posttranscriptionally up-/downregulated had significantly higher/lower protein abundance, respectively (P = 1.38e-03 and 9.11e-03; Supplementary Material). Of special interest are the activity state predictions of moderately expressed reactions, whose activity state is left undetermined in the gene expression input provided for MPA. Indeed, those moderately expressed reactions that were predicted via MPA to be active have a significantly higher protein abundance than those that were predicted to be inactive (P = 9.58e-04).

Breast cancer progression is accompanied by reduced proliferation associated with oxidative stress

Following its validation, we used MPA profiles generated for 392 breast cancer clinical samples on the basis of their gene expression (24, 32) to study the metabolic alterations that accompany breast cancer progression. As expected, the MPA biomass scores, an approximation of the proliferation capacity of the cell, are significantly higher in advanced grades than in early ones (Wilcoxon rank-sum P = 1.088e-02). However, the MPA biomass scores decrease with increased metastatic potential as depicted by the tumor stage (P = 4.06e-02). Concomitantly, the capacity to biosynthesize essential metabolites as lipids and nucleotides is decreasing in advanced stages (Supplementary Table S6).

We turned to study this intriguing prediction of proliferation deceleration in a combined computational experimental manner. We used a panel of breast cancer cell lines that were extracted from 2 premalignant tumors, 1 stage II tumor, 2 stage III tumors, and 2 metastasis cells from pleural effusions. Together, this panel provides a view of the transformation process toward the metastatic phenotype. The elevated tumorigenic potential of these cells with increased stage has been previously shown experimentally in combination with a global proteomic analysis (35). Measurement of the growth rates of these cells showed statistically significant differences between cells from different stages (ANOVA P = 9.40e-04). The premalignant cells have a significantly higher growth rate than stage II, stage III, and the cells from metastases (with P = 1.61e-03, 7.63e-03, 6.72e-08, respectively), whereas stage II cells have a significantly higher growth rate than metastasis ones (P = 3.31e-02). We computed the MPA biomass scores for these breast cancer cell lines on the basis of their quantitative proteomics. The computational MPA biomass scores, obtained for the cell lines and for the clinical samples, as well as the experimental growth rate measurements, all exhibit the same trend: proliferation decreases with the disease progression.

The experimentally measured growth rates correlated with the MPA biomass scores (Spearman correlation = 0.7857, P = 4.80e-02; Fig. 2A). Notably, other extant CBM methods that were used to predict the proliferation rate [flux balance analysis (ref. 36) and the integrative metabolic analysis tool (iMAT); refs. 18, 27] failed to predict the observed growth rates (with correlation coefficients of −0.0187 and −0.1352, respectively). In difference from MPA, FBA does not account for the specific context-dependent gene expression or protein abundance of the modeled cells; iMAT does not account for the cells' potential to adaptively deviate from these context-dependent transcriptomic or proteomic signatures. Thus, iMAT may miss cellular metabolic responses that successfully maintain a given metabolic process but are infeasible while forcing a maximal fit to the given expression data. Conversely, MPA can successfully identify such responses by allowing for some relaxation of this fit. These differences can explain the superior performance of MPA in this task.

To trace the causes for the decrease in anabolic biomass production capacity, we returned to the clinical samples and computed the MPA scores of metabolic reactions in central metabolic processes: glycolysis, tricarboxylic acid (TCA) cycle, and the pentose phosphate pathway (PPP). On the basis of these scores we compared the metabolic functionality of early- and late-stage tumors. In accordance with the Warburg effect, the activity of glycolysis, lactate production, and PPP was higher in late-stage tumors (Fig. 2B; ref. 37). However, MPA showed that the products of PPP are not used for synthesizing fatty acids and nucleotides. Instead, they are diverted to the detoxification of ROS: late-stage tumors have a higher capacity to detoxify ROS than early-stage ones (one-sided Wilcoxon rank-sum P = 6.161e-3), and proliferation and *de novo* lipogenesis are negatively correlated to ROS detoxification capacity (Spearman correlation coefficient of −0.639 and −0.574, respectively; Fig. 2C and D).

The observed tradeoff between proliferation and ROS detoxification can be partially explained by competition over the consumption of NADPH, which is a shared limiting resource for these processes (Fig. 3). Following this, superoxide levels were measured in metastatic breast cancer cells (MDA-MB-453 and MFM223) and nonmetastatic cells (HCC1143 and HCC1937). The metastatic cell lines show significantly lower levels of superoxide, suggesting that the predicted increase in shunting of NADPH to the mitochondria indeed successfully manages to counteract the predicted increase in ROS production (Supplementary Fig. S4). Overall, these results indicate that as the disease progresses toward metastasis formation, the resources of the tumor are increasingly used to counteract oxidative stress, limiting the activity of anabolic processes, and hence, hindering proliferation (Fig. 3).

ER^+ metabolism versus ER^- metabolism

While reduced proliferation and increase ROS detoxification were identified as general phenomena in breast cancer progression, we sought to examine metabolic differences between the ER^- and ER^+ breast cancer subtypes. MPA indicates that the metabolism of ER^+ tumors is considerably different than that of ER^- tumors, with approximately 73% of the metabolic processes having significantly different MPA scores (Wilcoxon $P < 0.05$; Supplementary Table S7). In accordance with the literature, we find that glutamine biosynthesis and secretion is significantly higher in ER^+ (Wilcoxon P = 1.84e-02), whereas serine metabolism and glutamine uptake are significantly

Published OnlineFirst on September 17, 2012; DOI:10.1158/0008-5472.CAN-12-2215

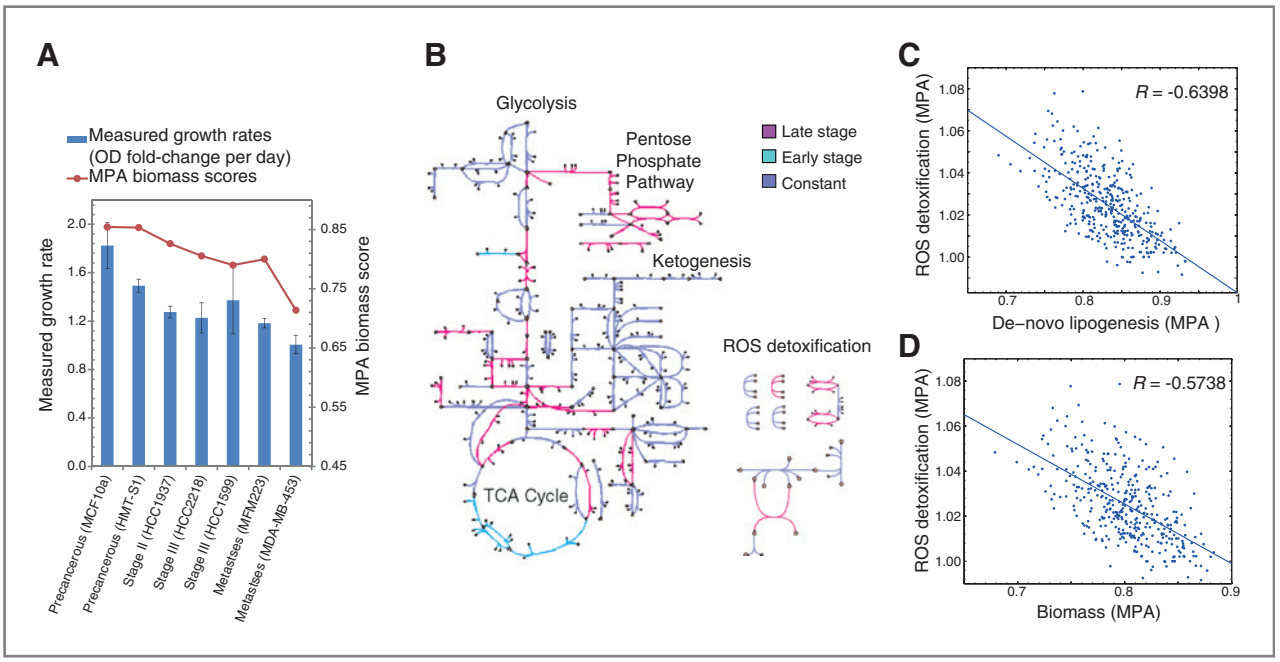

Figure 2. MPA predicts that proliferation is decelerating, while ROS detoxification is increasing with breast cancer progression. A, the average measured (blue bars) and MPA-predicted (red plot) growth rates of the different breast cancer cell lines, ordered according to their stage. B, the differences between the central metabolism of early- and late-stage tumors according to MPA. The MPA scores of the reactions colored in azure (pink) are significantly higher in early (late)-stage tumors. C and D, plots of the MPA ROS detoxification scores as a function of *de novo* lipogenesis (C) and biomass scores (D).

higher in ER^- ($P = 2.41e\text{-}10$ and 1.85e-17, respectively; Fig. 4A; refs. 7, 8). In addition, according to MPA, ER^+ tumors have a higher capacity to produce lactate from glucose than ER^- tumors ($P = 1.70e\text{-}2$), probably as in ER^- tumors 3-phosphoglycerate (3PG) is diverted toward serine metabolism via PHGDH (Fig. 4B). What underlies these distinct metabolic "signatures"? A sampling-based stoichiometric analysis (38) of the generic human metabolic model (9) reveals a fundamental tradeoff between serine and glutamine metabolism that arises due to pure stoichiometric constraints–the latter results in a negative correlation of −0.664 between the flux rates of glutamine secretion and serine metabolism (Fig. 4; Supplementary Material), in agreement with recent findings, showing that glutamine is the nitrogen donor for serine biosynthesis [phosphohydroxythreonine aminotransferase (PSAT1) transamination activity; ref. 7].

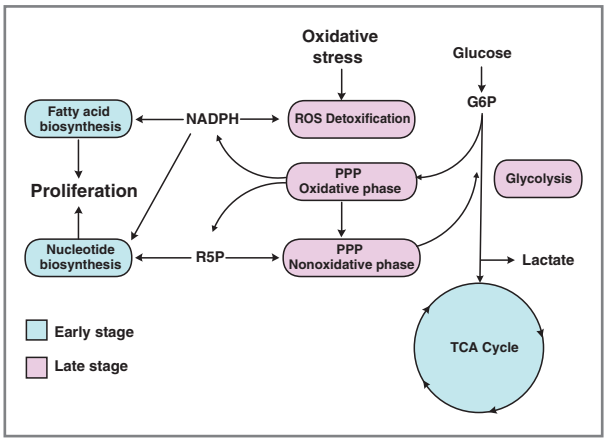

Figure 3. A systematic view of breast cancer metabolic progression according to MPA. A pathway-level description of the differences between the metabolism of early- and late-stage tumors, as suggested by MPA. In azure (pink) are processes that are more active in early (late)-stage tumors.

Biomarker identification in metastatic breast cancer

MPA was used to predict biomarkers for metastatic breast cancer. Initially, its ability to conduct this task was validated by applying it to predict amino acids biomarkers for breast cancer, based on the gene expression of patients with breast cancer and controls (22–24). The predictions were compared with a set of breast cancer amino acid biomarkers (25). In accordance with the measurement, the predictions of MPA showed the reduction in the level of tyrosine, phenylalanine, histidine, and tryptophan, and the increase in the level of proline and glycine in the plasma of patients with breast cancer. The predictions of MPA matched the experimental measurements (accuracy of 0.588, with an empirical $P = 0.048$), whereas those obtained using iMAT did not (accuracy of 0.235, $P = 0.8432$). We then applied MPA to identify potential biomarkers for metastatic breast cancer. The top predicted biomarkers of MPA (Supplementary Table S8) are 2 choline-containing metabolites (lysophosphatidylcholine and phosphatidylcholine), which are predicted to be more highly consumed by the metastatic tumors than by the nonmetastatic ones (FDR-corrected Wilcoxon rank-sum $P = 4.45e\text{-}02$). Interestingly, choline has been suggested as a potential positron emission tomographic (PET) marker for imaging breast cancer (39), and a recent review of cancer biomarkers lists choline and

Published OnlineFirst on September 17, 2012; DOI:10.1158/0008-5472.CAN-12-2215

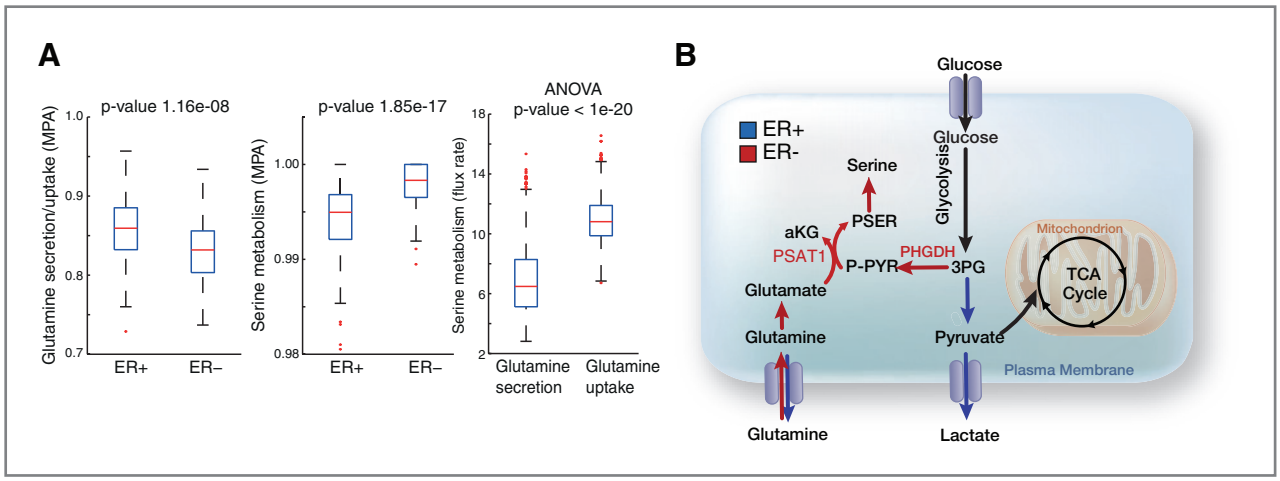

Figure 4. ER$^-$ and ER$^+$ breast cancer differ in glutamine and serine metabolism. A, the MPA scores of glutamine uptake/secretion (right) and PHGDH (middle) computed for ER$^+$ and ER$^-$ tumors. The flux rate of PHGDH under glutamine uptake or secretion, according to sampled flux distributions (right). B, a metabolic network, depicting differences between ER$^+$ and ER, as manifested in the MPA scores. aKG, α-ketoglutarate; P-PYR, 3-phosphohydroxypyruvate; PSER, phosphoserine.

phosphocholine as 2 of the 6 well-established biomarkers of breast cancer (40). Furthermore, the rate of choline transport under physiological choline concentrations has been reported to be 2-fold higher in the breast cancer cell lines than in normal mammary epithelial cells (41).

Discussion

Here, we present the first genome-scale computational study of breast cancer metabolism. The study reveals a basic distinction between the proliferative and invasive phenotypes. This "go or grow" dichotomy has been previously shown in glioma (42, 43) and melanoma (44, 45) and has been indicated by small-scale mathematical models of cancer behavior (46, 47). Our results suggest that this phenomenon is of broader context and holds also in breast cancer. Evidently, it has been shown that breast cancer subpopulations with elevated metastatic activity are not more proliferative than their parental population (48). In agreement, the levels of circulating but nonproliferating breast cancer cells are positively correlated with bone marrow metastasis (49). Nonetheless, as our pertaining results were obtained in cell lines, an experimental *in vivo* validation is still required to fully substantiate this trend.

MPA suggests a mechanistic explanation for the "go or grow" phenomenon: The growing need of the metastatic cancer cells to counteract oxidative stress necessarily hinders their proliferation, due to the growing need to funnel NADPH from lipogenesis to ROS detoxification. This mechanism adds upon the ones attributed to the Warburg effect (37), by which the cancer cells reduce the level of ROS. The need to detoxify ROS can be partially explained by the nonapoptotic death process that prevents the survival of matrix-deprived cells (50). It has been shown that matrix-deprived cells can be rescued either by stimulating the flux through the antioxidant-generating PPP or through the direct administration of antioxidants (6). This selection for cells with improved antioxidant capacities is reflected in our results and elucidates the need of the cancer cells to reduce their proliferation to survive. The tradeoff between ROS detoxification and proliferation highlighted here is expected to be more general, as it is caused by intrinsic stoichiometric constraints of the metabolic network. It has been recently reported that an increase both in lipogenesis and in ROS levels is associated with apoptosis (51), supporting the hypothesis that overproduction of lipids, as required for proliferation, hampers the capacity to detoxify ROS.

MPA's mapping of the metabolic differences between ER$^+$ and ER$^-$ tumors mirrors and elucidates recent experimental observations. Serine metabolism was found here to be stoichiometrically coupled to glutamine uptake, providing a potential explanation for its exclusive essentiality in ER$^-$ tumors. In accordance, MPA indicates that ER$^-$ tumors have a lower capacity to produce lactate from glucose, suggesting they operate other mechanisms to oxidize NADH, such as glutaminolysis. These results show how stoichiometry can explain the different metabolic routes taken by ER$^+$ and ER$^-$ tumors. It is likely that such stoichiometric couplings are more general, and their identification and potential role in determining specific cancer metabolic subtypes awaits further study.

The computational experimental study presented here provides new insights into the metabolic progression of breast cancer, revealing both generic and subtype-specific metabolic characteristics. It paves the way for a system-level understanding of breast cancer metabolism that is cardinal for its diagnosis and treatment. Considering the success of our computational approach in capturing different aspects of breast cancer metabolism, it opens up many additional possibilities for the genome-scale study of breast cancer metabolism in particular and cancer metabolism in general.

Disclosure of Potential Conflicts of Interest

E. Ruppin has ownership interest (including patents) for a patent submitted on drug discovery in cancer. No potential conflicts of interest were disclosed by the other authors.

Published OnlineFirst on September 17, 2012; DOI:10.1158/0008-5472.CAN-12-2215

Authors' Contributions

Conception and design: L. Jerby, G.Y. Stein, T. Geiger, E. Ruppin
Development of methodology: L. Jerby, L. Wolf, E. Ruppin
Acquisition of data (provided animals, acquired and managed patients, provided facilities, etc.): C. Denkert, M. Hilvo, M. Oresic, T. Geiger
Analysis and interpretation of data (e.g., statistical analysis, biostatistics, computational analysis): L. Jerby, G.Y. Stein, M. Hilvo
Writing, review, and/or revision of the manuscript: L. Jerby, C. Denkert, M. Hilvo, M. Oresic, T. Geiger, E. Ruppin
Administrative, technical, or material support (i.e., reporting or organizing data, constructing databases): L. Jerby, C. Denkert, M. Oresic
Conducted the proliferation and ROS measurement experiments and provided the proteomics of the breast cancer cell lines: T. Geiger
Provided data of lipid measurements and gene expression profiling of breast cancer biopsies: C. Denkert, M. Hilvo, M. Oresic

Grant Support

L. Jerby is partially funded by the Edmond J. Safra bioinformatics program and the Dan David foundation. The research of T. Geiger and E. Ruppin is supported by the Israeli Centers of Research Excellence (I-CORE), Gene Regulation in Complex Human Disease Center No 41/11. The research of E. Ruppin is supported by grants from the Israeli Science Foundation (ISF) and the Israeli Cancer Research Fund (ICRF).

The costs of publication of this article were defrayed in part by the payment of page charges. This article must therefore be hereby marked *advertisement* in accordance with 18 U.S.C. Section 1734 solely to indicate this fact.

Received June 9, 2012; revised August 6, 2012; accepted September 1, 2012; published OnlineFirst September 17, 2012.

References

1. Ward Patrick S, Thompson Craig B. Metabolic reprogramming: a cancer hallmark even Warburg did not anticipate. Cancer cell 2012; 21:297–308.
2. Tennant DA, Duran RV, Gottlieb E. Targeting metabolic transformation for cancer therapy. Nat Rev Cancer 2010;10:267–77.
3. Hanahan D, Weinberg Robert A. Hallmarks of cancer: the next generation. Cell 2011;144:646–74.
4. Cancer: metabolic link to breast cancer. Nature 2010;468:478.
5. Di L-J, Fernandez AG, De Siervi A, Longo DL, Gardner K. Transcriptional regulation of BRCA1 expression by a metabolic switch. Nat Struct Mol Biol 2010;17:1406–13. Available from: http://www.nature.com/nsmb/journal/v17/n12/abs/nsmb.1941.html#supplementary-information.
6. Schafer ZT, Grassian AR, Song L, Jiang Z, Gerhart-Hines Z, Irie HY, et al. Antioxidant and oncogene rescue of metabolic defects caused by loss of matrix attachment. Nature. 2009;461:109–13. Available from: http://www.nature.com/nature/journal/v461/n7260/suppinfo/nature08268_S1.html.
7. Possemato R, Marks KM, Shaul YD, Pacold ME, Kim D, Birsoy K, et al. Functional genomics reveal that the serine synthesis pathway is essential in breast cancer. Nature. 2011;476:346–50. Available from: http://www.nature.com/nature/journal/v476/n7360/abs/nature10350.html#supplementary-information.
8. Kung H-N, Marks JR, Chi J-T. Glutamine synthetase is a genetic determinant of cell type-specific glutamine independence in breast epithelia. PLoS Genet 2011;7:e1002229.
9. Duarte NC, Becker SA, Jamshidi N, Thiele I, Mo ML, Vo TD, et al. Global reconstruction of the human metabolic network based on genomic and bibliomic data. Proc Natl Acad Sci U S A 2007;104:1777–82.
10. Segre D, Vitkup D, Church GM. Analysis of optimality in natural and perturbed metabolic networks. Proc Natl Acad Sci U S A 2002; 99:15112–7.
11. Kumar VS, Maranas CD. GrowMatch: an automated method for reconciling *in silico*/*in vivo* growth predictions. PLoS Comput Biol 2009;5:e1000308.
12. Papp B, Notebaart RA, Pál C. Systems-biology approaches for predicting genomic evolution. Nat Rev Genet 2011;12:591–602.
13. Kim HU, Sohn SB, Lee SY. Metabolic network modeling and simulation for drug targeting and discovery. Biotechnol J 2012;7: 330–42.
14. Bordbar A, Palsson BO. Using the reconstructed genome-scale human metabolic network to study physiology and pathology. J Intern Med 2012;271:131–41.
15. Shlomi T, Cabili MN, Ruppin E. Predicting metabolic biomarkers of human inborn errors of metabolism. Mol Syst Biol 2009;5:263.
16. Folger O, Jerby L, Frezza C, Gottlieb E, Ruppin E, Shlomi T. Predicting selective drug targets in cancer through metabolic networks. Mol Syst Biol 2011;7:501.
17. Frezza C, Zheng L, Folger O, Rajagopalan KN, MacKenzie ED, Jerby L, et al. Haem oxygenase is synthetically lethal with the tumour suppressor fumarate hydratase. Nature 2011;477:225–8. Available from: http://www.nature.com/nature/journal/v477/n7363/abs/nature10363.html#supplementary-information.
18. Shlomi T, Cabili MN, Herrgard MJ, Palsson BO, Ruppin E. Network-based prediction of human tissue-specific metabolism. Nat Biotechnol 2008;26:1003–10.
19. Mahadevan R, Schilling CH. The effects of alternate optimal solutions in constraint-based genome-scale metabolic models. Metab Eng 2003;5:264–76.
20. Available from: https://cs.tau.ac.il/~livnatje/MPA.zip [cited 2012 Jul].
21. Benjamini Y, Hochberg Y. Controlling the false discovery rate: a practical and powerful approach to multiple testing. J R Stat Soc Ser B (Methodological) 1995;57:289–300.
22. Turashvili G, Bouchal J, Baumforth K, Wei W, Dziechciarkova M, Ehrmann J, et al. Novel markers for differentiation of lobular and ductal invasive breast carcinomas by laser microdissection and microarray analysis. BMC Cancer 2007;7:55.
23. Graham K, de las Morenas A, Tripathi A, King C, Kavanah M, Mendez J, et al. Gene expression in histologically normal epithelium from breast cancer patients and from cancer-free prophylactic mastectomy patients shares a similar profile. Br J Cancer 2010;102:1284–93. Available from: http://www.nature.com/bjc/journal/v102/n8/suppinfo/6605576s1.html.
24. Chang HY, Nuyten DSA, Sneddon JB, Hastie T, Tibshirani R, Sørlie T, et al. Robustness, scalability, and integration of a wound-response gene expression signature in predicting breast cancer survival. Proc Natl Acad Sci U S A 2005;102:3738–43.
25. Miyagi Y, Higashiyama M, Gochi A, Akaike M, Ishikawa T, Miura T, et al. Plasma free amino acid profiling of five types of cancer patients and its application for early detection. PLoS One 2011;6:e24143.
26. Akesson M, Forster J, Nielsen J. Integration of gene expression data into genome-scale metabolic models. Metab Eng 2004;6:285–93.
27. Zur H, Ruppin E, Shlomi T. iMAT: an integrative metabolic analysis tool. Bioinformatics 2010;26:3140–2.
28. Becker SA, Palsson BO. Context-specific metabolic networks are consistent with experiments. PLoS Comput Biol 2008;4:e1000082.
29. Jensen PA, Papin JA. Functional integration of a metabolic network model and expression data without arbitrary thresholding. Bioinformatics 2011;27:541–7.
30. Gille C, Bolling C, Hoppe A, Bulik S, Hoffmann S, Hubner K, et al. HepatoNet1: a comprehensive metabolic reconstruction of the human hepatocyte for the analysis of liver physiology. Mol Syst Biol 2010;6:411. Available from: http://www.nature.com/msb/journal/v6/n1/suppinfo/msb201062_S1.html.
31. Hilvo M, Denkert C, Lehtinen L, Müller B, Brockmöller S, Seppänen-Laakso T, et al. Novel theranostic opportunities offered by characterization of altered membrane lipid metabolism in breast cancer progression. Cancer Res 2011;71:3236–45.
32. van 't Veer LJ, Dai H, van de Vijver MJ, He YD, Hart AA, Mao M, et al. Gene expression profiling predicts clinical outcome of breast cancer. Nature 2002;415:530–6.
33. Staiger C, Cadot S, Kooter R, Dittrich M, Müller T, Klau GW, et al. A critical evaluation of network and pathway-based classifiers for outcome prediction in breast cancer. PLoS One 2012;7:e34796.
34. Nagaraj N, Wisniewski JR, Geiger T, Cox J, Kircher M, Kelso J, et al. Deep proteome and transcriptome mapping of a human cancer cell

Published OnlineFirst on September 17, 2012; DOI:10.1158/0008-5472.CAN-12-2215

line. Mol Syst Biol 2011;7:548. Available from: http://www.nature.com/msb/journal/v7/n1/suppinfo/msb201181_S1.html.

35. Geiger T, Madden SF, Gallagher WM, Cox J, Mann M. Proteomic portrait of human breast cancer progression identifies novel prognostic markers. Cancer Res 2012;72:2428–39.
36. Varma A, Palsson BO. Metabolic flux balancing: basic concepts, scientific and practical use. Bio Technol 1994;12:994–8.
37. Hsu PP, Sabatini DM. Cancer cell metabolism: Warburg and beyond. Cell 2008;134:703–7.
38. Becker SA, Feist AM, Mo ML, Hannum G, Palsson BO, Herrgard MJ. Quantitative prediction of cellular metabolism with constraint-based models: the COBRA Toolbox. Nat Protocol 2007;2:727–38. Available from: http://www.nature.com/nprot/journal/v2/n3/suppinfo/nprot.2007.99_S1.html.
39. Zheng Q-H, Stone KL, Mock BH, Miller KD, Fei X, Liu X, et al. [11C]choline as a potential PET marker for imaging of breast cancer athymic mice. Nuclear Med Biol 2002;29:803–7.
40. Davis VW, Bathe OF, Schiller DE, Slupsky CM, Sawyer MB. Metabolomics and surgical oncology: potential role for small molecule biomarkers. J Surgical Oncol 2011;103:451–9.
41. Katz-Brull R, Seger D, Rivenson-Segal D, Rushkin E, Degani H. Metabolic markers of breast cancer. Cancer Res 2002;62:1966–70.
42. Giese A, Loo MA, Tran N, Haskett D, Coons SW, Berens ME. Dichotomy of astrocytoma migration and proliferation. Int J Cancer 1996;67:275–82.
43. Giese A, Bjerkvig R, Berens ME, Westphal M. Cost of migration: invasion of malignant gliomas and implications for treatment. J Clin Oncol 2003;21:1624–36.
44. Haqq C, Nosrati M, Sudilovsky D, Crothers J, Khodabakhsh D, Pulliam BL, et al. The gene expression signatures of melanoma progression. Proc Natl Acad Sci U S A 2005;102:6092–7.
45. Hoek KS, Eichhoff OM, Schlegel NC, Döbbeling U, Kobert N, Schaerer L, et al. *In vivo* switching of human melanoma cells between proliferative and invasive states. Cancer Res 2008;68:650–6.
46. Hatzikirou H, Basanta D, Simon M, Schaller K, Deutsch A. 'Go or Grow': the key to the emergence of invasion in tumour progression? Math Med Biol 2012;29:49–65.
47. Fedotov S, Iomin A. Migration and proliferation dichotomy in tumor-cell invasion. Phys Rev Lett 2007;98:118101.
48. Kang Y, Siegel PM, Shu W, Drobnjak M, Kakonen SM, Cordón-Cardo C, et al. A multigenic program mediating breast cancer metastasis to bone. Cancer Cell 2003;3:537–49.
49. Müller V, Stahmann N, Riethdorf S, Rau T, Zabel T, Goetz A, et al. Circulating tumor cells in breast cancer: correlation to bone marrow micrometastases, heterogeneous response to systemic therapy and low proliferative activity. Clin Cancer Res 2005;11:3678–85.
50. Mailleux AA, Overholtzer M, Schmelzle T, Bouillet P, Strasser A, Brugge JS. BIM regulates apoptosis during mammary ductal morphogenesis, and its absence reveals alternative cell death mechanisms. Dev Cell 2007;12:221–34.
51. Boren J, Brindle KM. Apoptosis-induced mitochondrial dysfunction causes cytoplasmic lipid droplet formation. Cell Death Differ 2012;19:1561–70. Available from: http://www.nature.com/cdd/journal/vaop/ncurrent/suppinfo/cdd201234s1.html.